

Age-dependent Mortality, Fecundity, Mobility Effects on the Neolithic Transition

Joaquim Pérez-Losada
 Complex Systems Laboratory, Department of Physics
 Universitat de Girona
 Girona, Spain 17071
 Email: joaquim.perez@udg.edu

Abstract—We present a model that makes it possible to analyze the effect of the age dependences of mortality, fertility and dispersal persistence on the speed of propagating fronts in two spatial dimensions. Speeds derived analytically agree very well with those obtained from numerical simulations. Infant mortality and total fecundity are the most relevant parameters affecting the front speed, whereas the adult mortality rates and dispersal persistences are less important. We apply the model to the Neolithic transition in Europe. The predictions of the model are consistent with the archaeological data for the front speed, provided that the infant mortality lies within a relatively narrow range.

I. INTRODUCTION

Reaction-dispersal front propagation models have been recently applied to many systems, such as human invasions [1], [2]. A variety of models has been developed in recent years to analyze the speeds of human invasion fronts [3]. Recently, the following integro-differential equation has been proposed (for some derivations, see Eq. (10) in Ref. [4], Eq. (4) and Fig. 1 in Ref. [5], and Eq. (176) and Fig. 17 in [6]),

$$p(x, y, t + T) = F \int_{-\infty}^{+\infty} \int_{-\infty}^{+\infty} p(x + \Delta_x, y + \Delta_y, t) \phi(\Delta_x, \Delta_y) d\Delta_x d\Delta_y, \quad (1)$$

where $p(x, y, t + T)$ is the population density at the location (x, y) and time $t + T$. The time interval T is that between two subsequent dispersal events or 'jumps', i.e. one generation (defined as the mean age difference between an individual and her/his children). The parameter F appearing in Eq. (1) is the net fecundity or reproductive rate (number children per parent which survive to adulthood). The dispersal kernel $\phi(\Delta_x, \Delta_y)$ is the probability per unit area that the children of an individual located at $(x + \Delta_x, y + \Delta_y, t)$ become adults at $(x, y, t + T)$. Strictly, Eq. (1) is valid at sufficiently low values of the population density p , because there is a maximum saturation density above which net reproduction vanishes (see Eq. (9) in Ref. [4]).

Equation (1) is called the non-overlapping generation model. Note that in this model, all traits in the life history of the individuals are ignored, i.e. only the age-independent parameters T and F are used. Therefore, this model cannot analyze any effect on the front speed of the fact that the

fecundity, mortality and dispersal kernel depend on the age of individuals. In this paper, we will extend this model to allow for such dependencies [7].

II. THE MODEL

In order to take into account the dependencies of fecundity, mortality and dispersal on age, we regard the population as subdivided into several age groups. For simplicity, and also for later application to data appropriate to the Neolithic transition (Sec. IV), we consider only four groups (however, all of our results can be easily extended to an arbitrarily large number of groups). For definiteness, let the age group subindices be ordered so that $p_1(x, y, t)$ corresponds to the youngest age group and $p_4(x, y, t)$ to the oldest one. Then we generalize Eq. (1) into the set

$$\left\{ \begin{array}{l} p_1(x, y, t + \tau) = f_2 \int \phi_2(\Delta_x, \Delta_y) p_2(x + \Delta_x, y + \Delta_y, t) d\Delta_x d\Delta_y \\ \quad + f_3 \int \phi_3(\Delta_x, \Delta_y) p_3(x + \Delta_x, y + \Delta_y, t) d\Delta_x d\Delta_y \\ \quad + f_4 \int \phi_4(\Delta_x, \Delta_y) p_4(x + \Delta_x, y + \Delta_y, t) d\Delta_x d\Delta_y \\ p_2(x, y, t + \tau) = (1 - m_1) \int \phi_1(\Delta_x, \Delta_y) p_1(x + \Delta_x, y + \Delta_y, t) d\Delta_x d\Delta_y \\ p_3(x, y, t + \tau) = (1 - m_2) \int \phi_2(\Delta_x, \Delta_y) p_2(x + \Delta_x, y + \Delta_y, t) d\Delta_x d\Delta_y \\ p_4(x, y, t + \tau) = (1 - m_3) \int \phi_3(\Delta_x, \Delta_y) p_3(x + \Delta_x, y + \Delta_y, t) d\Delta_x d\Delta_y \end{array} \right. \quad (2)$$

where $p_i(x, y, t)$ is the population density (number of individuals per unit area) of age-group i , f_i is its fecundity, m_i its mortality, and $\phi_i(\Delta_x, \Delta_y)$ its dispersal kernel. We assume that the infant population $p_1(x, y, t)$ does not reproduce, so that $f_1 = 0$ in Eqs. (2) (this is in agreement with the data we will use in Sec. IV). The time interval τ should be chosen so that the demographic data on mortality, fecundity and dispersal, which are always recorded in age intervals, can be applied

to Eqs. (2) (see Sec. III). Similarly to the age groups with densities p_1 , p_2 and p_3 , mortality will also affect the dynamics of subpopulation p_4 , but this effect is not included in Eqs. (2) for the following reason. Since by definition p_4 is the oldest age group, all individuals corresponding to p_4 will simply disappear after their reproduction and dispersal, and their death will not affect the front speed.

In order to derive the theoretical speed for our model, we look for constant-shape solutions for each subpopulation, i.e. $p_i(x, y, t) = w_i \exp[-\lambda(x - ct)]$ ($i=1,2,3$) in the limit in which the coordinate co-moving with front $z \equiv x - ct \rightarrow \infty$. Then the set of Eqs. (2) becomes

$$\begin{cases} w_1 \exp(\lambda c) = f_2 w_2 \int_0^\infty \varphi_2(\Delta) I_0(\lambda \Delta) \Delta d\Delta \\ \quad + f_3 w_3 \int_0^\infty \varphi_3(\Delta) I_0(\lambda \Delta) \Delta d\Delta \\ w_2 \exp(\lambda c) = (1 - m_1) w_1 \int_0^\infty \varphi_1(\Delta) I_0(\lambda \Delta) \Delta d\Delta \\ w_3 \exp(\lambda c) = (1 - m_2) w_2 \int_0^\infty \varphi_2(\Delta) I_0(\lambda \Delta) \Delta d\Delta, \end{cases} \quad (3)$$

where

$$I_0(\lambda \Delta) \equiv \frac{1}{2\pi} \int_0^{2\pi} d\theta \exp[\lambda \Delta \cos \theta] \quad (4)$$

is the modified Bessel function of the first kind and order zero, and we have assumed that ϕ_i depend only on distance $\Delta \equiv \sqrt{\Delta_x^2 + \Delta_y^2}$ (isotropic kernels). The dispersal probability per unit area $\phi_i(\Delta)$ is related to that per unit length $\varphi_i(\Delta)$ (i.e. into a 2D ring of area $2\pi\Delta d\Delta$) as $\varphi_i(\Delta) = 2\pi\Delta\phi_i(\Delta)$ [8].

For simplicity, let us assume a simple description in which

$$\phi_i(\Delta) = p_{ei} \delta^{(2)}(\Delta) + (1 - p_{ei}) \delta^{(2)}(\Delta - r) \quad (5)$$

where $\delta^{(2)}$ is the two-dimensional Dirac delta function, i.e., an individual of age group i either stays at rest (with probability p_{ei} , which is called the persistence of age group i) or moves distance r (with probability $1 - p_{ei}$). Such a description has been useful previously in several models [4], [5], [9] that did not take the age structure of the population into account. In those papers it was also shown that a realistic value for the mobility distance of prehistoric human populations is $r = 50$ km. We use a single value for r because using a different value for each age group would substantially complicate the simulations in Sec. III. We think this is reasonable because in our model the value of the persistence p_{ei} (and, therefore, the mobility behavior of the individuals) is allowed to depend on age. Then, using matrix notation, the system (3) can be rewritten as

$$\exp(\lambda c) \vec{w} \equiv \vec{H}(\lambda) \vec{w}, \quad (6)$$

where we have defined

$$\vec{w} \equiv \begin{pmatrix} w_1 \\ w_2 \\ w_3 \end{pmatrix}, \quad (7)$$

$$\vec{H}(\lambda) \equiv \begin{pmatrix} 0 & f_2 \Psi_2(\lambda) & f_3 \Psi_3(\lambda) \\ (1 - m_1) \Psi_1(\lambda) & 0 & 0 \\ 0 & (1 - m_2) \Psi_2(\lambda) & 0 \end{pmatrix}, \quad (8)$$

and

$$\Psi_i(\lambda) \equiv p_{ei} + (1 - p_{ei}) I_0(\lambda r). \quad (9)$$

As usual, according to marginal stability analysis [10] the front speed c for systems with the form (6) can be found from the well-known expression [11]

$$c = \min_{\lambda} \frac{1}{\lambda} \rho_1(\lambda), \quad (10)$$

with ρ_1 the largest of the eigenvalues of $\vec{H}(\lambda)$.

III. NUMERICAL SIMULATIONS

The numerical simulations of the system (2) are performed on a 2D grid with 1000 x 1000 nodes, with nearest-neighbors distance $r = 50$ km (see Sec. II). Initially $p_i(x, y, t) = 0.25$ (but the front speed does not depend on this value) for $i = 1, \dots, 4$ at the central node, and 0 elsewhere. At each time interval, corresponding to $\tau = 12.5$ yr, we compute the new subpopulation number densities $p_i(x, y, t + \tau)$ at all nodes of the 2D grid in a two-step process: dispersal and growth (the latter includes reproduction and deaths). In the dispersal step, as in the analytical model in Sec. II, a fraction p_{ei} of the population in age group i stays at the original node, and the remaining fraction is distributed equally among the nearest neighbors, i.e., a fraction $(1 - p_{ei})/4$ jumps a distance $\pm r$ along each horizontal or vertical direction. In the second step, the effects of reproduction and mortality are computed as follows. At each node, the new infant population density p_1 is computed as $\sum_{i=2}^4 f_i p_i$ (the numerical values of f_i are given below). The new population density p_i for each of the remaining three age groups ($i = 2, \dots, 4$) is computed by removing a fraction $m_{i-1} p_{i-1}$ to the population density p_{i-1} (see the last three equations in the set ((2)). In order to avoid an unbounded population growth, if after any of these steps a population density in a grid node exceeds the saturation value, then it is set equal to the saturation value (we used a saturation value of unity in our simulations, but changing it does not modify the front speed). The two-step dispersal-growth cycle is then repeated many times, until a constant speed for the propagation of the population profiles is reached.

The mean observed values of the parameters, as well as the ranges used in the simulations, are reported in Table 1. They have been obtained as follows. First, as mentioned above, in order to use the histograms for the fecundities in Refs. [12], [13], the appropriate interval between age groups is $\tau = 12.5$ yr. From table 2 in Ref. [12], the characteristic value for the total fertility ratio F of preindustrial agriculturalists was estimated as $F \simeq 6.6$ children per adult woman. The characteristic value of F is given in children per adult in our Table 1, as appropriate for application in our model (this is half the value per adult woman, because the number of women and men in human populations are approximately the same). An upper bound for F was set to 7.0 children per adult woman

TABLE I
 MODEL PARAMETERS AND THEIR RANGES

Parameter (units)	Value	Minim.	Max.	Refs.
F (children/adult)	3.30	3.00	3.50	[12] , [13]
m_1 (dimensionless)	0.55	0.27	0.77	[14]
m_2 (dimensionless)	0.30	0.15	0.45	[14]
m_3 (dimensionless)	0.40	0.20	0.60	[14]
m_4 (dimensionless)	1.00	1.00	1.00	[14]
p_{e1} (dimensionless)	0.38	0.19	0.54	[15]
p_{e2} (dimensionless)	0.38	0.19	0.54	[15]
p_{e3} (dimensionless)	0.38	0.19	0.54	[15]
p_{e4} (dimensionless)	0.38	0.19	0.54	[15]

(from the estimations for Linearbandkeramic (LBK) farmers during their range expansion in Western Europe [13]). The minimum value for preindustrial agriculturalists is $F = 6.0$ children per adult woman, according to table 2 in in Ref. [12]. The age-dependent fecundities f_i used in our model were estimated by multiplying the total fertility ratio F times the age-specific relative ratios (defined as the age-specific rate f_i divided by the total rate F) in natural fertility populations, as given in Ref. [13], Fig. 2.5. This yields $f_1 = 0.0$, $f_2 = 2.3$, $f_3 = 1.0$, $f_4 = 0.0$ children per women. Therefore, note that for a given value of F , the values of f_2 and f_3 are given by the equations $f_2/f_3 = 2.3$ and $f_2 + f_3 = F$. Age-dependent mortalities were estimated from table 4 in [14], yielding the characteristic values $m_1 = 0.55$, $m_2 = 0.30$, $m_3 = 0.40$, $m_4 = 1.00$. Finally, Ref. [15] is the only source we know with quantitative dispersal data for preindustrial agriculturalist populations. Unfortunately, it does not seem possible to estimate the age-dependent persistencies p_{ei} because all mobility data give individual distances moved since birth, not since the individual had several specific ages. However, Ref. [15] makes it possible to estimate several values of the infant persistence. As noted in a previous publication [4], the mean is $p_{e1} = 0.38$ and the range is $0.19 \leq p_{e1} \leq 0.54$. Due to the lack of more refined information, and because infants necessarily move with adults, we approximated the adult persistencies (p_{e2} , p_{e3} and p_{e4}) to the same range as that of p_{e1} (Table 1). Moreover, we will find that our model is consistent with the data for any value of the adult persistencies (Fig. 1).

IV. APPLICATION TO THE NEOLITHIC TRANSITION IN EUROPE

Finally we can apply our model to the Neolithic transition in Europe. In Fig. 1, the full lines are the analytical results from Eq. (10), and the symbols have been obtained using the numerical simulations described in the previous section. In Fig. 1, the persistence of the infant population p_{e1} has its mean observed value (Table 1) and we have assumed $p_{e2} = p_{e3}$ (because, as mentioned above, only p_{e1} can be reliably estimated from the ethnographic data available, whereas p_{e2} and p_{e3} cannot). The persistence of old adults p_{e4} does not have any effect on the front speed (simply because it appears only in the term multiplying $f_4 = 0$ in Eqs. (2)). The hatched

Pérez-Losada, Fig. 1

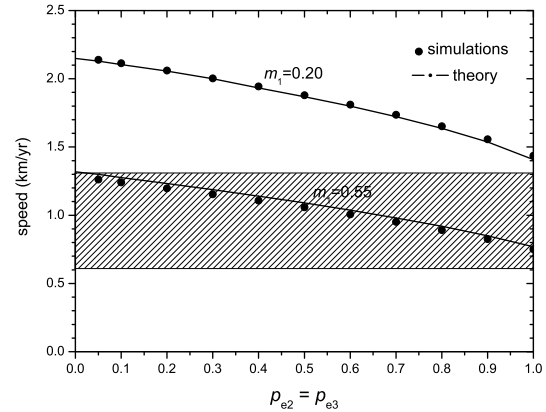


Fig. 1. Front speed in 2D versus adult dispersion persistence, for two values of the infant mortality. Adapted from [7].

rectangle corresponds to the speed range of the Neolithic transition in Europe, as determined from archaeological data (0.6 to 1.3 km/year) [16].

From Fig. 1 we see that the infant mortality m_1 has a very important effect on the front speed. Indeed, the predicted speeds are consistent with the observed range (hatched rectangle) for an infant mortality of $m_1 = 0.55$ (this value has been directly measured for some preindustrial populations, see table 4 in [14]). However, the predicted speeds are totally inconsistent with the observed range for other values of the infant mortality, e.g. for $m_1 = 0.20$. From Fig. 1 we conclude that (i) the predictions of the model are consistent with the observed speed range for realistic values of the infant mortality, and (ii) the role of the infant mortality should be taken into account in order to understand human invasion front speeds, as done here for the first time. In Fig. 1 we also note that the speed decreases with increasing values of the mortality, as was to be expected intuitively (if less people survive, less people can migrate and the front speed should be slower). Also, according to Fig. 1, the higher the value of the adult persistence ($p_{e2} = p_{e3}$), the slower the front propagates, as was again to be expected (less people migrate if the persistence is higher, see Sec. II). Finally, in Fig. 1 it is seen that the numerical simulations (circles) confirm the validity of our analytical results (curves).

It is important to estimate the importance of each parameter value on the front speed. In order to do so, in Fig. 2 we present a sensitivity analysis, performed as follows. All but one of the adjustable parameters were fixed at the characteristic value given in Table 1. The speed was then computed for the single remaining parameter set to its minimum and maximum values in Table 1. Figure 2 shows that the model is very sensitive to the infant mortality m_1 and, to less extent, to the total fecundity ratio F . The model is somewhat sensitive to the young adult mortality m_2 and to the persistencies of the

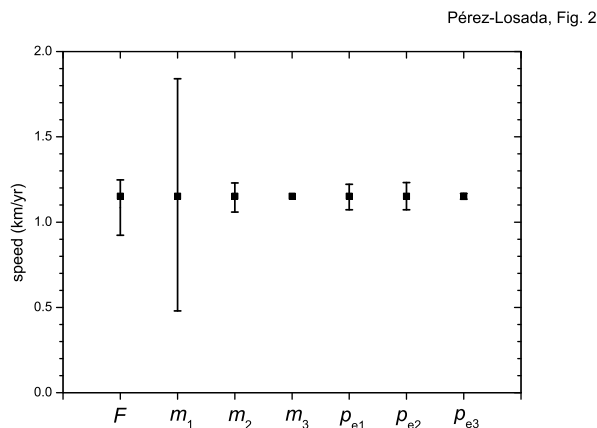


Fig. 2. Sensitivity analysis of the model as regards its parameter values. Adapted from [7].

infantiles (p_{e1}) and young adults (p_{e2}), albeit to a lesser extent. The persistence of the mature adults, p_{e3} , has a non-vanishing but a very small effect. Finally, the model is insensitive to the mortality of mature adults, m_3 . This was expected because, according to the ethnographic data [14], the oldest individuals (with density p_4) do not reproduce ($f_4 = 0$), so the last equation in the set (2) should not affect the propagation behavior of the front, and it is only in this equation that the parameter m_3 appears. Indeed, this expectation has made it possible to reduce Eqs. (2) to the simpler system, which in turn has lead us to our analytical result for the front speed [Eqs. (6)- (10)].

Finally, let us analyze in more detail the effect of infant mortality m_1 on the invasion front speed, given its importance (Fig. 2) as well as its novelty. Figure 3 shows this effect (when keeping the other parameters fixed at their baseline or characteristic values in Table 1). As in Fig. 1, the hatched rectangle shows the observed speed range for the Neolithic transition in Europe (0.6 to 1.3 km/year). Simulated values (rhombus) are in almost perfect agreement with theoretical ones (open circles and full curve). It is important to note that, according to Fig. 3, for the predicted speed to lie within the experimental range, the infant mortality must be rather high, $m_1 > 0.5$ (as is indeed observed in preindustrial populations [14]). Moreover, and quite interestingly, beyond a threshold value ($m_1 \simeq 0.63$ in Fig. 3) infant mortality is too high and the speed too slow compared to the range implied by the archaeological data (hatched rectangle). For even larger values of infant mortality, the front speed drops until it vanishes, thereby leading to a front propagation failure induced by infant mortality.

Although we have illustrated our model for a specific application (the Neolithic transition in Europe), clearly it can be also useful to other population expansions. Moreover, the effect of the mortality shown in Fig. 3 could be related to

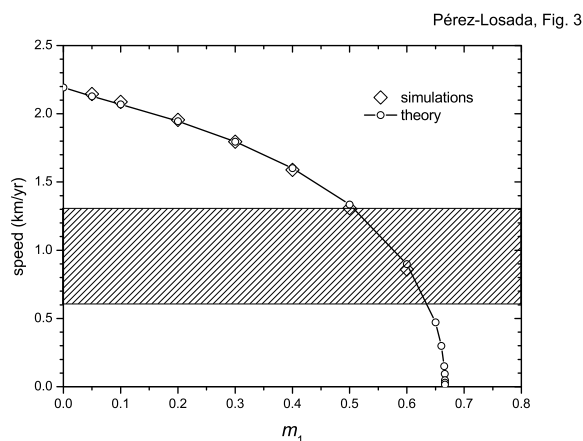


Fig. 3. The effect of infant mortality on the speed of the Neolithic transition. Adapted from [7].

several interesting factors. For example, a region with less natural resources (or a period of drought) could lead to higher values of the infant mortality m_1 , and thus to slower speeds (Fig. 3) or even to the failure of the invasive species (vanishing speed, also seen in Fig. 3) to successfully colonize the new habitat.

V. CONCLUSIONS

In this paper we have analyzed the effect of age-dependent mortality, fecundity and persistence on the invasion speed for populations that spread across a two-dimensional space. Our simulated and analytical front speeds are consistent with each other and, for realistic parameter ranges, with the observed speed of the Neolithic transition in Europe. Predicted speeds fall within the experimental range for realistic values of the infant mortality (e.g., $m_1 = 0.55$), and this conclusion is independent of the adult dispersal persistence (Fig. 1). The sensitivity of the results has been analyzed, with reference to a baseline case for the parameter values obtained from the ethnographic literature (Fig. 2). Infant mortality m_1 and total fecundity ratio F have the most important effects. This is the first model that relates the Neolithic front speed to the age-dependent demographic and dispersal parameters of the population. We have found that there is a relatively narrow range for the value of the infant mortality ($0.5 < m_1 < 0.63$) consistent with the observed range of the Neolithic front speed (Fig. 3). Of course, more complicated models can be considered, but for the application considered here it is very difficult to find more detailed ethnographic data, and our simple model takes into account the age dependency of the major demographic parameters.

ACKNOWLEDGMENT

This work was partially funded by the MINECO projects SimulPast (Consolider-CSD2010-00034), FIS-2009-13050 and FIS-2012-31307, and the Generalitat de Catalunya project 2014-SGR-36.

REFERENCES

- [1] J. Fort and V. Méndez, *Phys. Rev. Lett.* **82**, 867 (1999).
- [2] K. Davison, P. Dolukhanov, G. R. Sarson, and A. Shukurov, *J. Archaeol. Sci.* **33**, 641 (2006).
- [3] J. Steele, *Hum. Biol.* **81**, 121 (2009).
- [4] J. Fort, J. Pérez-Losada and N. Isern, *Phys. Rev. E* **76**, 031913 (2007).
- [5] N. Isern, J. Fort and J. Pérez-Losada, *J. Stat. Mech.: Theory and Experiment* **P10012**, 1-17 (2008).
- [6] J. Fort and T. Pujol, *Rep. Progr. Phys.* **71**, 086001 1 (2008).
- [7] J. Pérez-Losada and J. Fort, *J. Stat. Mech.: Theory and Experiment* **P11006**, 1-13 (2010).
- [8] J. Fort, *J. Appl. Phys.* **101**, 094701 (2007).
- [9] J. Fort, J. Pérez-Losada, J. J. Suñol, L. Escoda and J. M. Massaneda, *New J. Phys.* **10**, 043045 (2008).
- [10] U. Ebert and W. van Saarloos, *Physica D* **146**, 1 (2000).
- [11] M. Neubert and H. Caswell, *Ecology* **81**, 1613 (2000).
- [12] D.W. Sellen and R. Mace, *Curr. Anthropol.* 38(5) 878-889 (1997).
- [13] B. Bogin, *The growth of humanity* (Wiley-Loss, New York, 2001).
- [14] V. Eshed, A. Gopher, T.B. Gage and I. Hershkovitz, *Am. J. Phys. Anthropol.* **124**, 315-329 (2004).
- [15] J. Stauder, *The Majangir. Ecology and Society of a Southwest Ethiopian People* (Cambridge University Press, Cambridge, 1971).
- [16] R. Pinhasi R, J. Fort and A.J. Ammerman, *PLoS Biology* **3**, 2220-2228 (2005).